

RESEARCH ARTICLE

Low-Temperature Synthesis of Anatase TiO₂ Nanoparticles with Tunable Surface Charges for Enhancing Photocatalytic Activity

Ye Li^{1,3}, Zhenping Qin¹, Hongxia Guo^{2,3*}, Hanxiao Yang¹, Guojun Zhang¹, Shulan Ji^{1,3}, Tingying Zeng⁴

1. College of Environmental and Energy Engineering, Beijing University of Technology, Beijing, China, 2. College of Materials Science and Engineering, Beijing University of Technology, Beijing, China, 3. Beijing Key Laboratory for Green Catalysis and Separation, Beijing, PR China, 4. MIT, Elect. Res. Lab, Cambridge, Massachusetts, United States of America

*hxguo@bjut.edu.cn



click for updates

OPEN ACCESS

Citation: Li Y, Qin Z, Guo H, Yang H, Zhang G, et al. (2014) Low-Temperature Synthesis of Anatase TiO₂ Nanoparticles with Tunable Surface Charges for Enhancing Photocatalytic Activity. PLoS ONE 9(12): e114638. doi:10.1371/journal.pone.0114638

Editor: Vipul Bansal, RMIT University, Australia

Received: August 1, 2014

Accepted: November 12, 2014

Published: December 15, 2014

This is an open-access article, free of all copyright, and may be freely reproduced, distributed, transmitted, modified, built upon, or otherwise used by anyone for any lawful purpose. The work is made available under the Creative Commons CC0 public domain dedication.

Data Availability: The authors confirm that all data underlying the findings are fully available without restriction. All relevant data are within the paper.

Funding: This work was financially supported by National Natural Science Foundation of China (21176005), National technology support program of China (Project No., 2011BAE29B00). The funders had no role in study design, data collection and analysis, decision to publish, or preparation of the manuscript.

Competing Interests: The authors have declared that no competing interests exist.

Abstract

In this work, the positively or negatively charged anatase TiO₂ nanoparticles were synthesized via a low temperature precipitation-peptization process (LTPPP) in the presence of poly(ethyleneimine) (PEI) and poly(sodium4- styrenesulfonate) (PSS). X-ray diffraction (XRD) pattern and high-resolution transmission electron microscope (HRTEM) confirmed the anatase crystalline phase. The charges of the prepared TiO₂, PEI-TiO₂ and PSS-TiO₂ nanoparticles were investigated by zeta potentials. The results showed that the zeta potentials of PEI-TiO₂ nanoparticles can be tuned from +39.47 mV to +95.46 mV, and that of PSS-TiO₂ nanoparticles can be adjusted from -56.63 mV to -119.32 mV. In comparison with TiO₂, PSS-TiO₂ exhibited dramatic adsorption and degradation of dye molecules, while the PEI modified TiO₂ nanoparticles showed lower photocatalytic activity. The photocatalytic performances of these charged nanoparticles were elucidated by the results of UV-vis diffuse reflectance spectra (DRS) and the photoluminescence (PL) spectra, which indicated that the PSS-TiO₂ nanoparticles showed a lower recombination rate of electron-hole pairs than TiO₂ and PEI-TiO₂.

Introduction

Photocatalytic degradation is an efficient and economical method to totally decompose organic contaminants into benign substances [1–2]. Titanium dioxide

(TiO₂) nanocrystal has attracted much attention as a photocatalyst due to its photostability, nontoxicity, high activity and relatively low cost [3]. TiO₂ has three crystalline forms: rutile, anatase and brookite [4]. Anatase titania usually exhibits higher photocatalytic activity than rutile and brookite, owing to its higher density of localized states, the surface-adsorbed hydroxyl radicals and slower charge carrier recombination [5–7]. Much work has been reported for preparation of anatase TiO₂, such as thermolysis [8–9], sol-gel [10–11], ultrasonic technique [12], solvothermal [13] and hydrothermal method [14–15], by which the resulted particles have to be annealed at suitable temperature to obtain crystalline TiO₂ with anatase phases. The annealing process at relatively high temperature would inevitably lead to particles agglomeration and hence reduction of their specific surface area [16–17]. Therefore, the low temperature methods for preparation of anatase TiO₂ particles and films attract much attention, due to the fact that calcinations step can be eliminated. Mesoporous aggregates of anatase TiO₂ were obtained by controlled hydrolysis reaction of titanium tetrabutoxide in non-aqueous media, isopropanol, and then aging at ambient conditions for more than 120 days [18]. Gao et al. have synthesized the superfine TiO₂ nanocrystals with tunable anatase/rutile ratios in aqueous ethanol solution by “low temperature dissolution–reprecipitation process” (LTDRP) and solvothermal treatment [19]. Burunkaya et al. have prepared directly the anatase TiO₂ particles by hydrolyzing titanium ethoxide in alcohols solvent, such as ethanol, n-butanol and n-hexanol, followed by reflux at low temperature of 93 °C, without calcination step [20]. An anatase hydrosol has been obtained by acidic hydrolysis of titanium isopropoxide at room temperature [21–22], and the nanocrystalline TiO₂ films were prepared after adding surfactant into the hydrosol. However, all of these anatase TiO₂ particles or films have been prepared using titanium alkoxide or chloride in non-aqueous alcohol media.

Moreover, the TiO₂ suspension with a high degree of dispersion stability is considered one of the important factors during the photocatalytic processes [23–27]. Thus, modification of TiO₂ particles by polymers or surfactants, which combines unique properties of dissimilar components, would favor dispersing the suspension. Two ways have been used to modify TiO₂ particles: one is to introduce a surfactant or polymer to a preformed nanoparticle (post-synthesis) [23–24]; and the other is to incorporate surfactants or polymers simultaneously during nanoparticle synthesis (in situ synthesis) [25–27]. The anionic surfactant, such as sodium dodecylsulphate (SDS) and sodium dodecyl benzene sulfonate (SDBS), have been introduced into TiO₂ particles for promoting the dimerization of rhodamine B (RhB) and subsequent adsorption on the TiO₂ surface [26–29]. The nanosized titanium dioxide particles and charged polyelectrolytes (PEs), such as poly(allyl aminehydrochloride) (PAH) and poly(styrene sulfonate sodium) (PSS), have been alternatively assembled to form multilayer composite film for photodegradation of RhB under ultraviolet (UV) irradiation [30]. However, the charge controllability and the photocatalytic performance of the positive or negative TiO₂ particles modified by polyelectrolyte need further investigation.

In this work, the charge-tuned TiO₂ nanoparticles with pure anatase phase were synthesized via a low temperature precipitation-peptization process (LTPPP) under ambient condition. The water soluble titanium sulfate salt (Ti(SO₄)₂) was used as precursor to fabricate either positive or negative anatase TiO₂ nanoparticles in the presence of cationic or anionic polyelectrolytes (PEs). The charges of as-prepared nanoparticles, such as pure TiO₂, poly(ethyleneimine) (PEI)-TiO₂ or poly(sodium 4-styrenesulfonate) (PSS)-TiO₂, manifested by zeta potentials, were tuned by the variations of pH and the amount of the polyelectrolytes, respectively. Then, the photocatalytic activities of as-prepared TiO₂ nanoparticles were investigated by degradation of organic methylene blue (MB) and rhodamine B (RhB) dyes. The possible mechanism of the photocatalytic performance of the charged TiO₂ nanoparticles is proposed based on photoluminescence (PL) emission and UV-vis diffuse reflectance spectra (DRS). This work may provide an additive strategy to charge controllable TiO₂ nanoparticles, which would find new application in other fields, such as electrophoretic particles and the charged films or membrane [31–33], in addition to photocatalysis.

Experiments

2.1 Materials

Titanium sulfate (Ti(SO₄)₂), methenamine(C₆H₁₂N₄), nitric acid, ethanol (analytically pure), methylene blue (MB) and rhodamine B (RhB) dyes were provided by Beijing Chemical Factory (Beijing, China) and used without further purification. Poly(ethyleneimine) (PEI, Mw=750,000) and poly(sodium 4-styrenesulfonate) (PSS, Mw=70,000) were purchased from Sigma- Aldrich Co.,(St. Louis, MO, USA). Deionized water was used throughout this research.

2.2 Preparation of PEs-modified TiO₂ nanoparticles

The PEs-modified TiO₂ nanoparticles were obtained at low temperature precipitation-peptization process (LTPPP). The negatively charged TiO₂ nanoparticles modified by PSS were prepared as an example. Specifically, 2.4 g titanium sulfate, used as titanium precursor, was dissolved in 50 ml of deionized water; then PSS was added (titanium sulfate: PSS=1:0.15~1:0.05 mole ratio) under stirring at ambient condition until it thoroughly dissolved. Subsequently, the mixture containing titanium precursor and PSS was added into 50 mL of 2.7 wt% C₆H₁₂N₄ aqueous solution in dropwise of 0.5 mL/min under stirring, and meanwhile, the precipitation produced. After stirring for 1 h, the precipitates were collected and washed with ethanol and deionized water thoroughly. Then the precipitates slurry was dispersed into 0.3 mol/L HNO₃ aqueous solution, and refluxed for 3 h at 50 °C. Thus, the PSS modified TiO₂ (PSS-TiO₂) was obtained, after thoroughly washed by water and dried. The process for preparing PEI modified TiO₂ (PEI-TiO₂) was similar as that of PSS-TiO₂, using PEI instead of

PSS polyelectrolyte. As a comparison, pure TiO₂ nanoparticles were prepared in the same procedure without adding any additives.

2.3 Characterization

The crystallographic structures of the as-prepared nanoparticles were characterized by X-ray diffraction method on a D8 advance installation, (Bruker/AXS, Germany) using Cu–K α 1 ($\lambda=1.5406$ Å) radiation source. Scanning electron microscopy (SEM) (SU8020, Hitachi, Japan) was employed to observe the morphologies of the samples, and the EDX spectra of the corresponding region were obtained by the equipped Oxford EDX instruments and AZtec software. The microstructures of nanoparticles were explored by a high-resolution transmission electron microscope (HRTEM; JEM-2100, JEOL, Japan) equipped with an electron diffraction, operated at 200 KeV with LaB6 emission source of electrons. Zeta potentials and dimensions of the TiO₂ nanoparticles in aqueous water suspension were measured using Zeta Potential/Particle Sizer (NICOMPTM 380ZLS, USA), after ultrasonic for 60 min. The pH of the suspensions was adjusted using diluted HCl or NaOH solution.

The UV-vis diffuse reflectance spectra (DRS) were performed at room temperature on a UV-2450 instrument (SHIMADZU, Japan) in the range of 200 nm to 600 nm, with BaSO₄ as the standard reflectance sample. The characteristic adsorption of the particles was obtained by the intercept of the linear extrapolation to the λ axis and the band gap energy (E_g), given as a function of band edge (λ_g) as formula (1), according to reference [34–35].

$$E_g = \frac{1240}{\lambda_g} \quad (1)$$

The photoluminescence (PL) spectra excited at 320 nm were recorded by a RF-5301PC fluorescence spectrophotometer (SHIMADZU, Japan) under ambient condition.

2.4 The adsorption performance and photocatalytic activity of the nanoparticles

The adsorption performances of the as-prepared nanoparticles were investigated by UV-vis intensity of 10 mg/L of methylene blue (MB) solution [36]. Specifically, 100 mg of photocatalyst, pure TiO₂, PEI-TiO₂, or PSS-TiO₂, was added into 100 mL of Methylene blue (MB) solution of 10 mg/L of concentration, respectively. The resultant slurries were fully stirred in darkness for a given time. Then 5 mL of the suspension was taken out and centrifuged to remove the suspended solids within time intervals. The supernatant was subjected into the colorimetric ware for UV-vis analysis on a UV-vis spectrophotometer (UV-3200 MAPADA, Shanghai Mapada Instruments Co., Ltd., China).

The photocatalytic activity of the nanoparticles were evaluated by their photo degradation of 10 mg/L of methylene blue (MB) or rhodamine B (RhB) solution. A 500 W UV lamp (365 nm) was used as the light source, and its distance from the liquid level was 15 cm. The photo degradation on dyes begin after their sufficient adsorption on photocatalyst in darkness. In a typical procedure, 100 mg of photocatalytic particles was added into 100 mL of MB or RhB solution with 10 mg/L concentration, respectively. The resultant slurry was fully stirred in darkness until it reached adsorption/desorption equilibrium. Then, the suspension was placed under the irradiation of UV light. Within a given time, 5 mL of suspension were taken out and centrifuged to remove the suspended particles, and the supernatant was transferred into a colorimetric ware for UV-vis analysis on a UV-vis spectrophotometer (UV-3200 MAPADA, Shanghai Mapada Instruments Co., Ltd., China). The dye concentration was determined at a wavelength of 664 nm (for MB) and 554 nm (for RhB) and quantified by a standard calibration based on Beer-lambert's law. The photocatalytic activity of the samples was calculated according to $\eta = ((C_0 - C_t)/C_0) \times 100\%$, where η represents the degradation efficiency of dyes, C_0 (mg/L) and C_t (mg/L) represents the concentration of dye in the aqueous solution at time $t=0$ and t respectively.

Results and Discussions

3.1 Structure analysis on TiO₂ nanoparticles

The anatase TiO₂ nanoparticles were prepared by LTPPP method, including precipitation and peptization steps. First, the amorphous Ti(OH)₄ precipitation was obtained by hydrolysis of titanium sulfate in the presence of alkaline methenamine. Then, the Ti(OH)₄ precipitation was peptized by dehydration in HNO₃ solution media, due to that the strong acidic environment favored formation of the single-crystalline anatase crystal [37]. The crystalline phases of pure TiO₂ nanoparticles without any additives, peptized at temperature of 30°C, 40°C, 50°C, respectively, were first investigated by XRD patterns (Fig. 1). The XRD pattern of Fig. 1(a) showed an obvious wide peak at 2θ of 15.3–35.6° and the weak wide peak at 2θ of 42.4–52.3°, indicating the formation of amorphous crystal at relatively low temperature of 30°C. These two wide peaks become slightly narrowed in Fig. 1(b), indicating the formation of some primary crystallite grain, when the peptization was performed at 40°C. Then, the separate and sharp peaks at 2θ of 25.24°, 37.7°, 48.1°, 53.8°, 55.0°, 62.6°, 68.7°, 70.2° and 75.0° were observed in Fig. 1(c), corresponding to (101), (004), (200), (105), (211), (213), (116), (220) and (215) planes of anatase TiO₂ (JCPDS card No. 21-1272) [38], respectively. This indicated that the crystalline anatase nanoparticles were formed at temperature of 50°C. The size of pure TiO₂ crystalline was calculated about 4~6 nm by Scherrer equation [39]. The XRD patterns of the PEs modified nanoparticles at 50°C shown in Fig. 1(d) and Fig. 1(e) indicated the similar peaks at 2θ position as that of the pure anatase TiO₂. The average sizes of the PEI-TiO₂

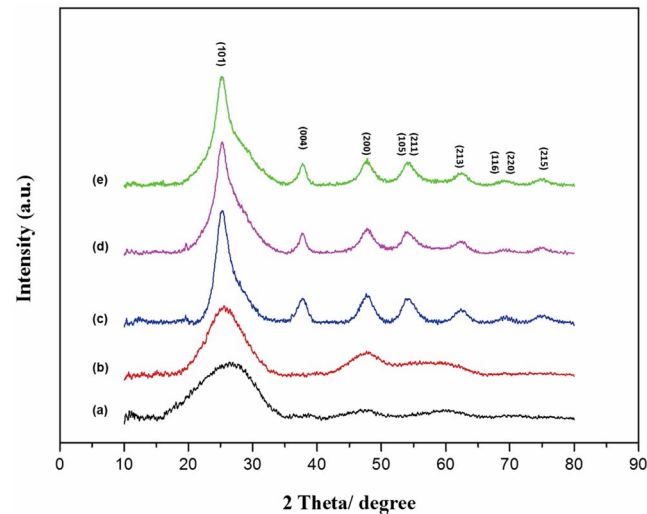


Fig. 1. XRD patterns of pure TiO₂ peptized at (a) 30°C, (b) 40°C and (c) 50°C; as well as the modified TiO₂ of (d) PSS-TiO₂ and (e) PEI-TiO₂.

doi:10.1371/journal.pone.0114638.g001

and PSS-TiO₂ crystallines were estimated as about 9.0~11.5 nm according to Scherrer equation.

[Fig. 2](#) showed the high-resolution transmission electron microscope (HRTEM) images of pure TiO₂, PEI-TiO₂ and PSS-TiO₂ nanoparticles. The enlarged TEM images in [Fig. 2](#) showed that all three nanocrystallites have lattice fringes of 0.356 nm, corresponding to (101) faces of anatase crystalline, indicating that the introduction of PEI and PSS polyelectrolytes into the precursor had little effect on lattice structure of TiO₂ crystal. Moreover, there were some amorphous regions in HRTEM images of [Fig. 2\(b\)](#) and [Fig. 2\(c\)](#), indicating that some immature crystalline in the presence of PEs. And the *d* spacing calculated from the electron diffraction pattern in the inset of [Fig. 2](#) matched the values of the three as-synthesized TiO₂ nanoparticles, which is in accordance with the consequence of XRD patterns of [Fig. 1](#).

The SEM morphologies of the particles shown in the inset on the right bottom of [Fig. 2](#) further manifested the overall morphology of nanoparticles. The SEM image of in [Fig. 2\(a\)](#) indicated that the pure TiO₂ nanoparticles clumped and aggregated together, with diameter ranged from ~200 to ~500 nm. In contrast, the PEs modified nanoparticles in [Fig. 2\(b\)](#) and [Fig. 2\(c\)](#) were relatively uniform spherical with diameter about ~150 nm to ~200 nm; interestingly, the PSS-TiO₂ nanoparticles were formed into some spherical bunched network. This indicated that the polyelectrolyte can reduce aggregation of the TiO₂ nanoparticle, effectively.

EDX measurements further demonstrated the PEs modification on TiO₂ particles. The existent elements on TiO₂, PEI-TiO₂ and PSS-TiO₂ nanoparticles were shown in the spectra of [Fig. 3](#), and the amounts of the elements were collected as in [Table 1](#). Besides of peaks of the sprayed Au (2.1 keV) and Si

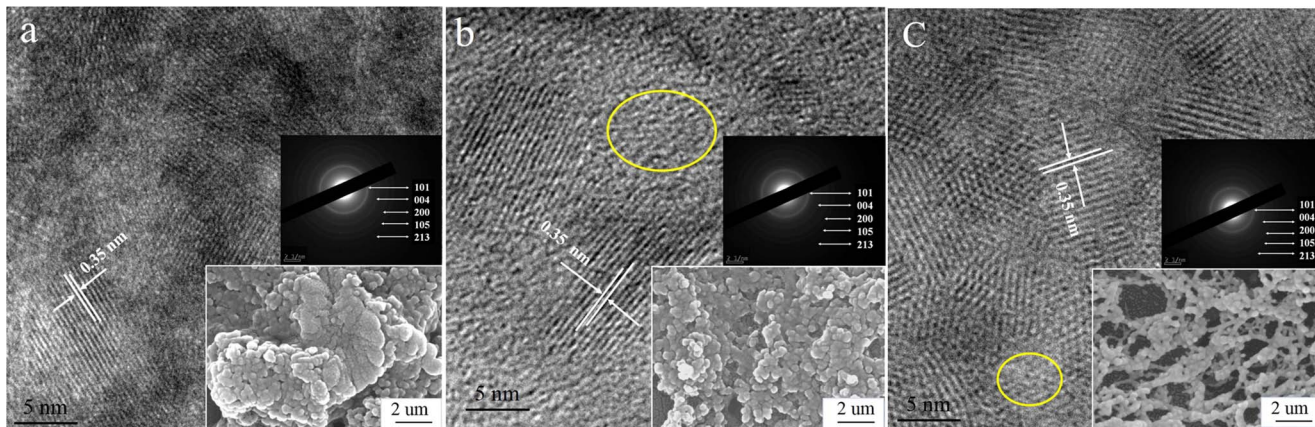


Fig. 2. High-resolution transmission electron microscope (HRTEM) images, SEM images, and the selected-area electron diffraction (SAED) patterns of (a) pure TiO₂, (b) PEI-TiO₂ and (c) PSS-TiO₂ nanoparticles.

doi:10.1371/journal.pone.0114638.g002

(1.7 keV) of the silicon substrate, [Fig. 3\(a\)](#) indicated two peaks of Ti elements (0.4 keV and 4.5 keV) and O elements (0.5 keV), indicating the characteristic constituent of TiO₂. In contrast, the new peaks of C (0.2 keV) and N (0.3 keV) elements in [Fig. 3\(b\)](#), and the peaks of C (0.2 keV), S (2.3 keV) and Na (1.0 keV) in [Fig. 3\(c\)](#) indicated obviously the existence of PEI and PSS on TiO₂ particles. The amounts of these elements shown in [Table 1](#) indicated that 29.22% of Ti and 70.78% of O were found on the pure TiO₂ nanoparticles; while there were 33.73%, 66.27%, 34.62% and 13.18% of Ti, O, C and N elements, respectively, existing on PEI-TiO₂ nanoparticle. Simultaneously, on PSS-TiO₂ nanoparticle, the amount of Ti, O, C, S and Na elements were 22.86%, 28.11%, 26.15%, 12.15% and 10.73%, respectively. This clearly indicated that the modification and existence of PEI or PSS on TiO₂ nanoparticles.

3.2 Zeta potential, particle size and dispersion stability of the nanoparticles suspension

[Fig. 4\(a\)](#) showed the variation of zeta potential of the nanoparticles with pH increasing from 3 to 11. The zeta potential of the PEI-TiO₂ nanoparticles showed gradual decrease, except for the slight increase of PEI-TiO₂ at pH of 5. The zeta potential of pure TiO₂ nanoparticles varied from +49.16 mV to -44 mV with iso-electric point at pH of 7, similar as that of pure anatase TiO₂ in Song's work [\[40\]](#). And zeta potential of the PSS-TiO₂ showed minus increase from -16 mV to -89.48 mV. This was partly ascribed to the enhanced adsorption of hydroxyl ions on surfaces of the nanoparticles, yielding significant increase on the negative charge, similar as the change of zeta potential with the adsorption of Cl⁻, NO₃⁻ and SO₄²⁻ [\[41\]](#). Moreover, the minus increase of zeta potential of TiO₂ nanoparticles with pH is attributed to the process shown in formula 2, the change of TiOH₂⁺ into TiO⁻ with pH increasing [\[28\]](#):

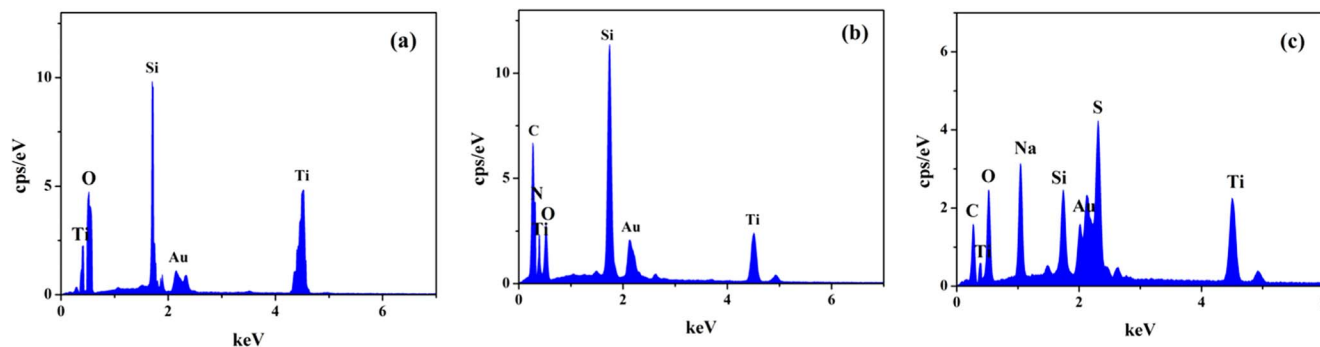
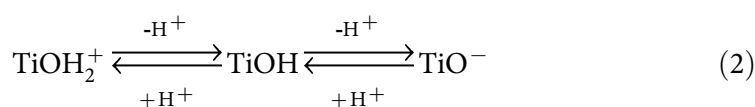


Fig. 3. EDX spectra of (a) TiO₂, (b) PEI-TiO₂ (10%) and (c) PSS-TiO₂ (10%).

doi:10.1371/journal.pone.0114638.g003



For the PEI-modified TiO₂ nanoparticles, the zeta potential showed a highest value of 69.85 mV at pH of 5.0. This was in accordance with the charge behavior of PEI, a weak polyelectrolyte, of which the amine groups were protonated in different level with pH [42], making it varied charges. As shown in the result of Fig. 4(b), the pure PEI showed a highest zeta potential at pH of 5, due to that its amine groups can be protonated enough at this pH value, resulting in the highest zeta potential of PEI-TiO₂. The zeta potential of PSS, a strong polyelectrolyte, was little affected by pH of the solution [43]. Thus, the zeta potential of PSS-TiO₂ is mainly dependent on the adsorptive abilities of hydroxyl ions on surfaces of nanoparticles with increase of pH, as well as the process shown in formula (2) [28], resulting in the highest zeta potential of -89.48 mV at pH of 11. Moreover, the variation of pH can also result in the change of the average dimension of the TiO₂, PEI-TiO₂ and PSS-TiO₂ nanoparticles. As shown in Fig. 4(c), the TiO₂ nanoparticles displayed largest average size at pH of 7, at which the zeta potential of the particle was zero (Fig. 4(a)). Thus, the almost no charged surface of the particles resulted in the aggregation more easily and with the largest aggregate size. In contrast, the PEI-TiO₂ particle displayed smallest size at pH of 5. This was probably due to that PEI-TiO₂ particle showed a highest zeta potential at pH of 5 (Fig. 4(a)), and the relatively strong electrostatic repulsion made the particles less

Table 1. The elemental amounts of TiO₂, PEI-TiO₂ (10%) and PSS-TiO₂ (10%) nanoparticles.

nanoparticles	Elements content (wt%)					
	Ti	O	C	N	S	Na
TiO ₂	29.22	70.78	0	0	0	0
PEI-TiO ₂	33.73	66.27	34.62	13.18	0	0
PSS-TiO ₂	22.86	28.11	26.15	0	12.15	10.73

doi:10.1371/journal.pone.0114638.t001

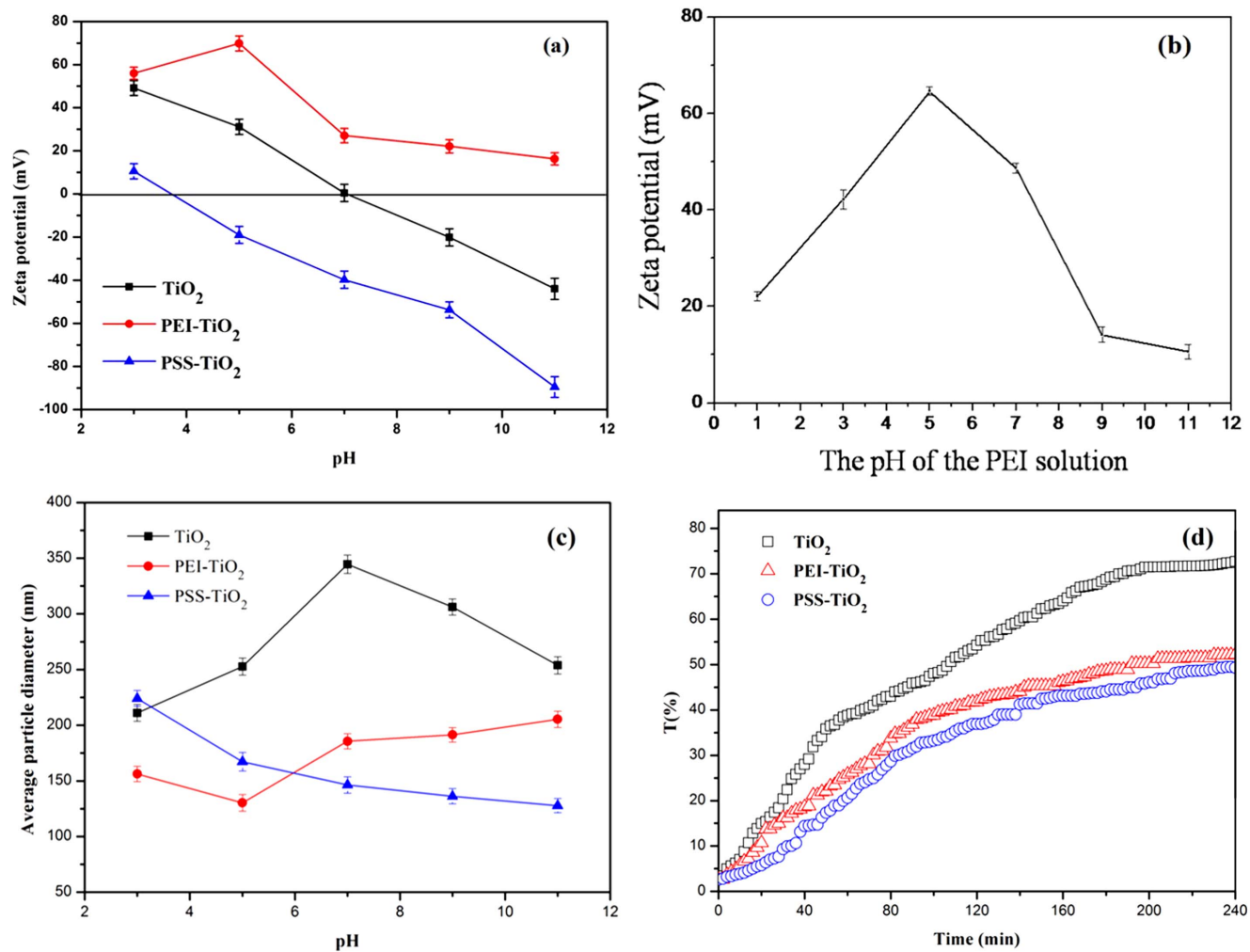


Fig. 4. Zeta potential of pure TiO₂, PEI-TiO₂ (10%) and PSS-TiO₂ (10%) as a function of pH (a); zeta potential of PEI (1.0 mg/mL) solution as a function of pH (b); Particle size of the TiO₂, PEI-TiO₂ and PSS-TiO₂ nanoparticles at different pH (c); Transmittance changes of TiO₂ (pH 3), PEI-TiO₂ (pH 5) and PSS-TiO₂ (pH 11) suspensions over time (d).

doi:10.1371/journal.pone.0114638.g004

aggregate and with smallest particle size. When pH value was greater than 5, the decreased zeta potential of PEI-TiO₂ (Fig. 4(a)) increased the chance of electrostatic attraction, and made the particles aggregate more easily and show the increased size. Similarly, the increased minus zeta potential of PSS-TiO₂ particles with pH resulted in the gradually decreased size. This indicated that the variation of the average size of the particles with pH was much in accordance with that of zeta potential.

The dispersion stability of TiO₂, PEI-TiO₂ and PSS-TiO₂ suspension were investigated by the variation of the suspension transmittance with time. The pH values of the three suspensions were 3, 5 and 11, respectively, in order to get a relatively higher charges and smaller aggregate size nanoparticles. As shown in Fig. 4(d), the transmittance of PEI-TiO₂ and PSS-TiO₂ suspensions displayed

slower increase with time than that of pure TiO₂ suspension, indicating that the relatively higher charges of nanoparticles can help to prompt the dispersion stability of the nanoparticles suspension.

In order to further achieve the tunable charge of nanoparticles, the variations of zeta potential with PEs concentration were investigated at pH value of the highest zeta potential of Fig. 4 (a). The results in Fig. 5 showed that the zeta potential of as-prepared PEI-TiO₂ nanoparticles at pH of 5 significantly increased from +39.47 mV to +95.46 mV with concentration of PEI increased from 1.0 wt% to 15.0 wt%. Meanwhile, the zeta potential of the PSS modified TiO₂ at pH of 11 showed obviously negative increase from -56.63 mV to -119.32 mV, with PSS concentration increased from 1.0 wt% to 15.0 wt%. The lower zeta potential of TiO₂ in the PSS solution is in accordance with that in SDS solution [27]. This can be explained by the hemimicelle model [44]. At high pH of 11, the negative PSS was adsorbed on the TiO₂ nanoparticle surface through physical adhesive interaction, causing the hemimicelle. When, PSS concentration increased, PSS micelles would be formed and adsorb on the TiO₂ nanoparticle surface, and the increased adsorption volumes resulted in more negative zeta potential [28]. The similar elucidation can also be illustrated for the change of zeta potential of PEI-TiO₂ with PEI concentration. The increases of zeta potential with the concentration of PEs indicated that the modification of polyelectrolyte of PEI or PSS on TiO₂ nanoparticles resulted in the tunable surface charge of the particles, effectively.

3.3 Adsorption and photocatalytic activity of nanoparticles

3.3.1 Adsorption of MB on the surface of nanoparticles

The adsorption of the organic substance on photocatalytic nanoparticles is considered as an important factor in their photocatalytic degradation. The adsorption performances of methylene blue (MB) on pure TiO₂, PEI-TiO₂, PSS-TiO₂ were investigated by the absorbance changes of UV-vis spectra of MB at given time in darkness. The slightly decreased absorbance of UV-vis spectra in Fig. 6 (a) indicated that there was weak adsorption of MB on TiO₂, which had little charges at pH of 7. And the absorbance the PEI-TiO₂ suspension in Fig. 6 (b) showed almost no change, indicating the negligible adsorption of MB on positively charged TiO₂. This was probably due to that the electrostatic repulsion between the positively charged PEI-TiO₂ nanoparticles and the positively charged MB. In contrast, the absorbance of MB in Fig. 6 (c) showed obvious decrease indicating that there was more MB adsorbed on negatively charged PSS-TiO₂ nanoparticles. This was due to that the positively charged MB was prone to adsorb on the negatively charged PSS-TiO₂ through electrostatic attraction, which may favor the next photocatalytic process.

3.3.2 Photocatalytic degradation of MB and RhB

Methylene blue (MB) is often used as a model contaminant of water for photocatalytic reaction test. And rhodamine B (RhB) is a typically industrial dye.

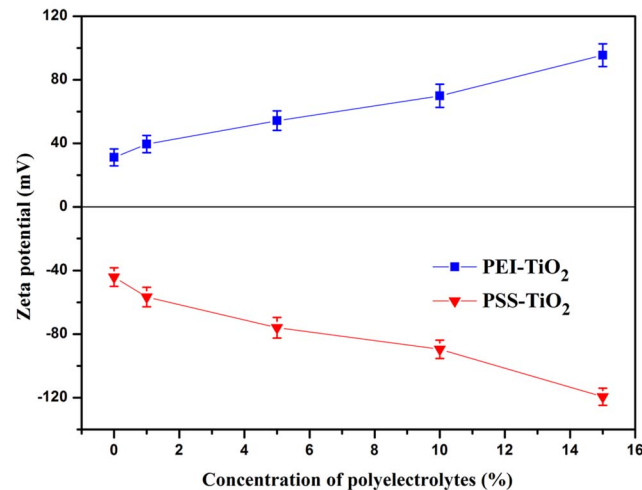


Fig. 5. The variations of zeta potentials of PEI-TiO₂ and PSS-TiO₂ nanoparticles with concentration of polyelectrolytes (pH of PEI-TiO₂ and PSS-TiO₂ was 5 and 11, respectively).

doi:10.1371/journal.pone.0114638.g005

The photodegradation was started after the thorough adsorption of dyes onto the photocatalyst in darkness. And the decolorization of dyes occurred with ultraviolet irradiation time. As shown in Fig. 7, the degradation efficiency on MB and RhB by photocatalysts, such as PEI-TiO₂, PSS-TiO₂ and TiO₂, were much similar, that is, the degradation efficiency of PSS-TiO₂ higher than that of TiO₂. And the degradation efficiency of PEI-TiO₂ is relatively lower than that of TiO₂. Fig. 7 (a) showed that 0.96 degradation efficiency of PSS-TiO₂ was observed on MB dye, a little higher than 0.95 and 0.84 of the pure TiO₂ and PEI-TiO₂, respectively, within 260 min of UV-light irradiation. Moreover, the PSS-TiO₂ photocatalyst exhibited more efficient photo-degradation on MB in the initial stage. For example, 0.67 of MB was degraded by PSS-TiO₂ within 20 min. In contrast, only 0.30 and 0.09 of MB were degraded by pure TiO₂ and PEI-TiO₂ photocatalysts within the same time. Fig. 7 (b) showed the similar results of

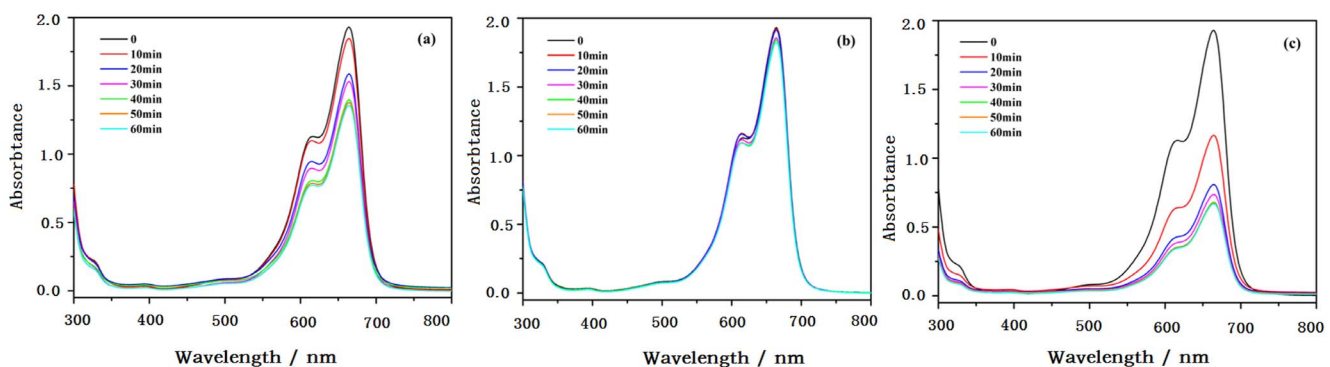


Fig. 6. UV-vis spectra of MB by the adsorption on (a)TiO₂, (b) PEI-TiO₂ and (c) PSS-TiO₂.

doi:10.1371/journal.pone.0114638.g006

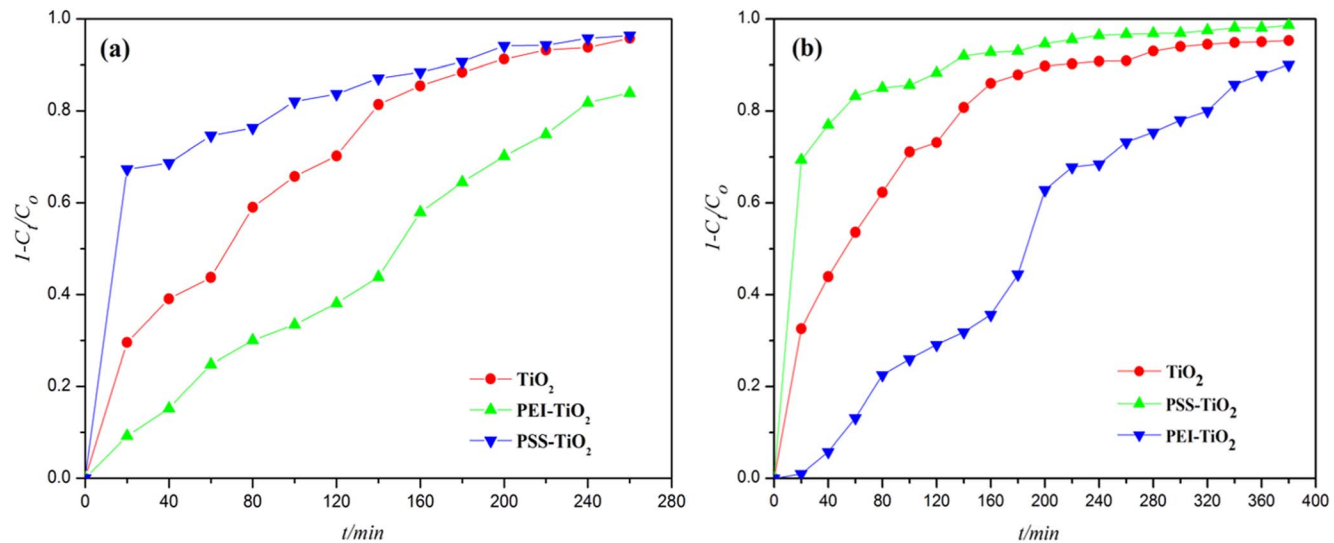


Fig. 7. Photocatalytic degradation with time under UV light in the presence of TiO₂, PEI-TiO₂ and PSS-TiO₂ photocatalysts of: (a) Methylene blue; (b) Rhodamine B.

doi:10.1371/journal.pone.0114638.g007

degradation of RhB. The degradation efficiency of RhB was about 0.90, 0.95 and 0.99 with PEI-TiO₂, TiO₂ and PSS-TiO₂, respectively, within 360 mins. This indicated that PSS-TiO₂ nanoparticles showed relatively higher photocatalytic activity. The possible reason is that the negatively charged PSS-TiO₂ easily adsorbed the positively charged MB by electrostatic attraction, as shown in Fig. 6(c), and made it effectively degraded. The relative lower degradation activity of MB over PEI-TiO₂ than pure TiO₂ nanoparticles is mainly ascribed to the electrostatic repulsion for MB shown in Fig. 6(b). For degradation of the RhB molecule, which contains both positively charged diethylamine groups and negatively charged carboxylate group, the carboxylate group is easily to adsorb onto Ti sites of TiO₂ surface [45]. While, the positively charged diethylamine groups are prone to interact electrostatically with negative species, such as PSS anion occupied on TiO₂ surface. Therefore, PSS-TiO₂ exhibited notably accelerated degradation rate of RhB.

3.3.3 Analysis of the photocatalytic performance of the nanoparticles

Generally, the electrons of TiO₂ would transfer from the valence band (VB) to conduction band (CB), when irradiated by photoelectrons with energy equal to/or larger than that of the band gap (E_g). Then, the photogenerated oxidative valence holes (h^+) and reductive conduction electrons (e^-) were produced [46]. In order to further expound the different photocatalytic performance of the above three samples, UV-vis diffuse reflectance spectra (DRS) were measured over the wavelength range from 200 nm to 600 nm. From the characteristic adsorption bands shown in Fig. 7, the band edge (λ_g) and band gap energy (E_g) of TiO₂, PEI-TiO₂ and PSS-TiO₂ photocatalysts were shown in Table 2. Generally, TiO₂ has a relatively high energy band gap ($E_g \approx 3.2$ eV) that can be excited under UV

Table 2. Band edge (λ_g) and band gap energy (E_g) of TiO₂, PEI-TiO₂ and PSS-TiO₂ photocatalysts.

Sample	λ_g /nm	E_g /eV
TiO ₂	499.0	2.88
PEI-TiO ₂	464.5	2.67
PSS-TiO ₂	621.36	2.44

doi:10.1371/journal.pone.0114638.t002

irradiation [47]. Here, the pure TiO₂ sample showed the typical adsorption of anatase with an intense transition in the UV region of the spectrum, which was due to the promotion of the electron from the valence band to the conduction band in Fig. 8. The energy band gap was calculated about 2.88 eV as in Table 2. This E_g was further lowered to 2.44 eV by PSS modification of TiO₂, in which the spectra band of the PSS-TiO₂ nanoparticles exhibited red shift in the UV-vis range of 300–500 nm. This red shift indicated that the PSS with π -conjugated structure of aromatic ring has high electron mobility [48]. The high photodegradation of dye molecules in Fig. 7 may be attributed to the efficient charge separation of the electrons (e⁻) and hole (h⁺) pairs at the interfaces of PSS and TiO₂ which is related to the red shift. However, the spectra band of PEI modified TiO₂ exhibited a blue shift with larger E_g of 2.67 eV. This blue shift is possibly due to n- σ^* transition of imine (-NH) in PEI macromolecules [49]. Consequently, the narrow band gap of PSS-TiO₂ in Fig. 7 made it an enhanced photocatalytic efficiency of TiO₂ under UV-light.

The photoluminescence (PL) emission, resulted from the recombination of excited electrons and holes further indicated the different photocatalytic efficiency as shown in Fig. 9. The broad-band emission spectra at around 375–410 nm are attributed to the luminescence signal, which indicated that the polyelectrolyte modification just affected the response range and intensity of the PL spectra, not causing new luminescence phenomenon in the PEI-TiO₂ and PSS-TiO₂

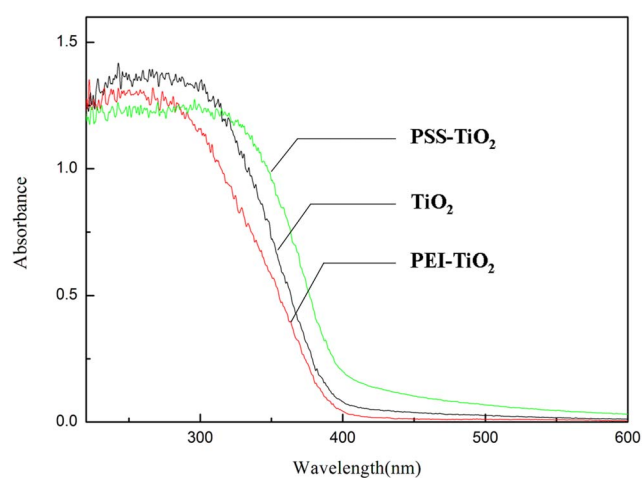


Fig. 8. UV-vis diffuses reflectance spectra of TiO₂, PEI-TiO₂ and PSS-TiO₂ photocatalysts.

doi:10.1371/journal.pone.0114638.g008

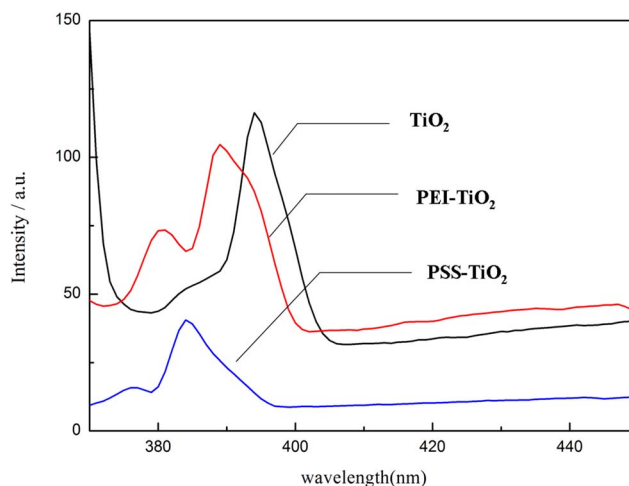


Fig. 9. PL emission spectra (excited at 320 nm) of TiO₂, PEI-TiO₂ and PSS-TiO₂ photocatalysts.

doi:10.1371/journal.pone.0114638.g009

nanoparticles. In comparison with that of pure TiO₂, the peak at about 396 nm for pure TiO₂ was attributed to the excitation luminescence of free electrons from the CB bottom. After PSS modification, the PL intensity of TiO₂ nanoparticles is significantly decreased, indicating that the PSS modification lowered recombination rate of electron/hole of TiO₂ samples. However, the PEI-TiO₂ nanoparticles displayed the higher PL intensity, indicating the higher recombination rate and E_g than PSS-TiO₂. This difference was also probably due to the E_g differences between π - π^* transition of PSS and the n - σ^* transition of imine (-NH) group of PEI polyelectrolyte, in accordance with that in [Table 2](#).

For better understanding of the photocatalytic activity differences between PEI-TiO₂ and PSS-TiO₂ photocatalysts, we used schemes of [Fig. 10](#) to illustrate the dye degradation over the photocatalysts surfaces. [Fig. 10 \(a\)](#) indicated that PSS with aromatic groups showed higher electron mobility, while the VB position of TiO₂ was lower than the highest occupied molecular orbital (HOMO) of PSS. Therefore, the hole (h^+) was easily formed by e^- electron transference from VB of TiO₂ to HOMO of PSS for e^- regeneration when TiO₂ absorbed UV light. The generated e^- from PSS can be excited from HOMO to the lowest unoccupied molecular orbital (LUMO) of PSS, and then the excited e^- transferred to the CB of TiO₂. Thus, more and more photogenerated e^- and h^+ formed on TiO₂ nanoparticles. The photogenerated e^- was so active that it can react with O₂ to generate $\cdot O_2^-$. Meanwhile, the generated h^+ can react with OH⁻ or H₂O to generate $\cdot OH$. These radicals would react with dye molecules, and produce organic radicals or other intermediates. Finally, the radicals and intermediates were oxidized into CO₂ and H₂O. PSS of the TiO₂ nanoparticles participated in charge transferring and favored enhancing the photocatalytic activities: e^- moved to the opposite direction from h^+ , reducing the recombination of photogenerated e^- - h^+ and making charge separation more efficient. The photogenerated e^- - h^+ pairs would favor the charge separation and the formation

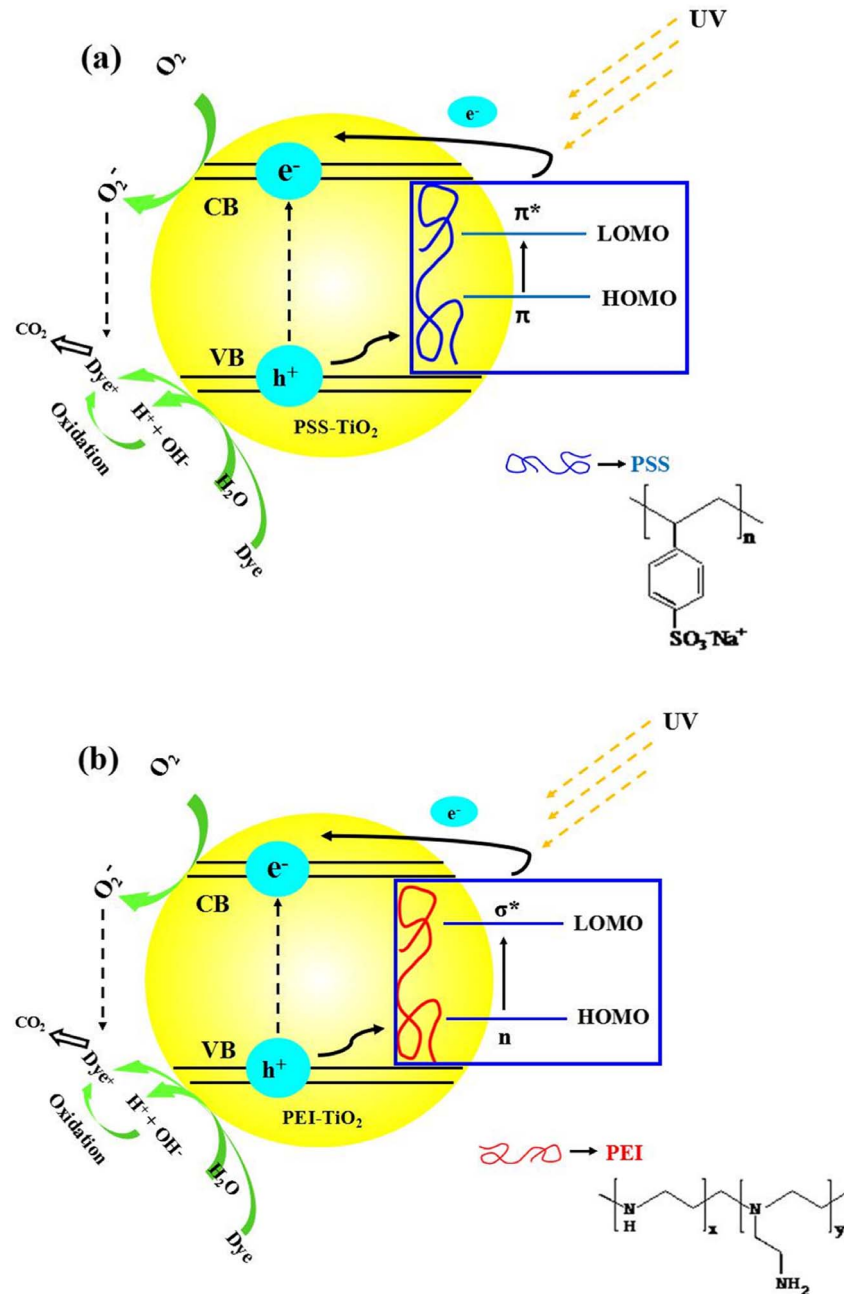


Fig. 10. Schematic illustration of photocatalytic activity of (a) PSS-TiO₂, (b) PEI-TiO₂ nanoparticles for dye degradation under UV-light.

doi:10.1371/journal.pone.0114638.g010

of oxyradicals (O₂^{•-}, OH[•]). Compared to PSS-TiO₂, the transition energy of n-σ* of PEI was much higher than that of π-π* of PSS, as shown in Fig. 10 (b). Hence, the negatively charged PSS-TiO₂ exhibited better photocatalytic activity than pure TiO₂ and positively charged PEI-TiO₂.

Conclusions

In conclusion, the anatase TiO₂ nanoparticles were prepared by simple method of LTPPP, under a room temperature and atmospheric pressure. The modification of PEI and PSS has little effect on the anatase crystallite phase of TiO₂. The zeta potential of nanoparticles can be effectively tuned by the variation of pH and the amount of polyelectrolytes during the synthesis process. Furthermore, PSS modified TiO₂ nanoparticles exhibited the highest degradation efficiency of Methylene blue and Rhodamine B, in comparison with pure TiO₂ and PEI-TiO₂ nanoparticles. The higher photocatalytic activity of the PSS-TiO₂ was attributed to the well adsorption of dye molecules, the reduced band gaps and lower recombination rate of electron/hole. This work would provide a simple and facile strategy to obtain various TiO₂-based functional materials, for which is of significance to extending the practical applications.

Author Contributions

Conceived and designed the experiments: HG. Performed the experiments: YL HY. Analyzed the data: YL ZQ GZ. Wrote the paper: YL HG TZ. Contributed all the characterization condition: SJ.

References

1. **Tayade RJ, Kulkarni RG, Jasra RV** (2006) Transition metal ion impregnated mesoporous TiO₂ for photocatalytic degradation of organic contaminants in water. *Ind Eng Chem Res* 45: 5231–5238. DOI: 10.1021/ie051362o
2. **Gaya UI, Abdullah AH** (2008) Heterogeneous photocatalytic degradation of organic contaminants over titanium dioxide: A review of fundamentals, progress and problems, *J Photoch Photobio C* 9:1–12. DOI: 10.1016/j.jphotochemrev.2007.12.003
3. **Liu N, Chen XY, Zhang JL, Schwanka JW** (2014) A review on TiO₂-based nanotubes synthesized via hydrothermal method: Formation mechanism, structure modification, and photocatalytic applications, *Catal Today* 225: 34–51. DOI: 10.1016/j.cattod.2013.10.090
4. **Khataee AR, Kasiri MB** (2010) Photocatalytic degradation of organic dyes in the presence of nanostructured titanium dioxide: Influence of the chemical structure of dyes, *J Mol Catal A: Chem* 328:8–26. DOI: 10.1016/j.molcata.2010.05.023
5. **Wang S, Lian JS, Zheng WT, Jiang Q** (2012) Photocatalytic property of Fe doped anatase and rutile TiO₂ nanocrystal particles prepared by sol-gel technique, *Appl Surf Sci* 263:260–265. DOI: 10.1016/j.apsusc.2012.09.040
6. **Zhang WF, Zhang MS, Yin Z, Chen Q** (2000) Photoluminescence in anatase titaniumdioxide nanocrystals, *Appl Phys B* 70:261–265. DOI:10.1007/s003409900161
7. **Xie MZ, Jing LQ, Zhou J, Lin JS, Fu HG** (2010) Synthesis of nanocrystalline anatase TiO₂ by one-pot two-phase separated, hydrolysis-solvothermal processes and its high activity for photocatalytic degradation of rhodamine B, *J Hazard Mater* 176:139–145. DOI: 10.1016/j.jhazmat.2009.11.008
8. **Cassaignon S, Koelsch M, Jolivet JP** (2007) Selective synthesis of brookite, anatase and rutile nanoparticles: thermolysis of TiCl₄ in aqueous nitric acid, *J Mater Sci* 42: 6689–6695. DOI: 10.1007/s10853-007-1496-y
9. **Agnès P, Chanèac C, Tronc E, Lèo M, Jolivet JP** (2001) Synthesis of brookite TiO₂ nanoparticles by thermolysis of TiCl₄ in strongly acidic aqueous media, *J Mater Chem* 11: 1116–11. DOI: 10.1039/b100435m

10. **Kumaresan L, Mahalakshmi M, Palanichamy M, Murugesan V** (2010) Synthesis, Characterization, and Photocatalytic Activity of Sr²⁺ Doped TiO₂ Nanoplates, *Ind Eng Chem Res.* 49: 1480–1485. DOI: 10.1021/ie901191z
11. **Li GS, Li LP, Boerio GJ, Woodfield BF** (2005) High Purity Anatase TiO₂ nanocrystals: near room-temperature synthesis, grain growth kinetics, and surface hydration chemistry, *J Am Chem Soc* 127: 8659–8666. DOI: 10.1021/ja050517g
12. **Wu XM, Wang L, Tan ZC, Li GH, Qu SS** (2001) Preparation, characterization, and low-temperature heat capacities of nanocrystalline TiO₂ ultrafine powder, *J Solid State Chem* 156: 220–224. DOI: 10.1006/jssc.2000.8991
13. **Zhang YC, Yang M, Zhang GH, Dionysiou DD** (2013) HNO₃-involved one-step low temperature solvothermal synthesis of N-doped TiO₂ nanocrystals for efficient photocatalytic reduction of Cr(VI) in water, *Appl Phys B* 142–143 249–258. DOI: 10.1016/j.apcatb.2013.05.023
14. **Nian JN, Teng H** (2006) Hydrothermal synthesis of single-crystalline anatase TiO₂ nanorods with nanotubes as the precursor, *J Phys Chem B* 110:4193–4198. DOI: 10.1021/jp0567321
15. **Thapa R, Maiti S, Rana TH, Maiti UN, Chattopadhyay KK** (2012) Anatase TiO₂ nanoparticles synthesis via simple hydrothermal route: Degradation of Orange II, Methyl Orange and Rhodamine B, *J Mol Catal A: Chem.* 363–364: 223–229. DOI: 10.1016/j.molcata.2012.06.013
16. **Zhang HZ, Banfield JF** (2000) Understanding polymorphic phase transformation behavior during growth of nanocrystalline aggregates: Insights from TiO₂, *J Phys Chem B* 104: 3481–3487. DOI: 10.1021/jp000499j
17. **Finnegan MP, Zhang HZ, Banfield JF** (2007) Phase stability and transformation in titania nanoparticles in aqueous solutions dominated by surface energy, *J Phys Chem C* 111: 1962–1968. DOI: 10.1021/jp063822c
18. **Deshpande SB, Potdar HS, Kholam YB, Patil KR, Pasricha R, et al.** (2006) Room temperature synthesis of mesoporous aggregates of anatase TiO₂ nanoparticles, *Mater Chem Phys* 97: 207–212. DOI: 10.1016/j.matchemphys.2005.02.014
19. **Gao Y, Wang H, Wu J, Zhao R, Lu YF, et al.** (2014) Controlled facile synthesis and photocatalytic activity of ultrafine high crystallinity TiO₂ nanocrystals with tunable anatase/rutile ratios, *Appl Surf Sci* 294: 36–41. DOI: 10.1016/j.apsusc.2013.12.107
20. **Burunkaya E, Akarsu M, Çamurlu HE, Kesmez O, Yeşil Z, et al.** (2013) Production of stable hydrosols of crystalline TiO₂ nanoparticles synthesized at relatively low temperatures in diverse media, *Appl Surf Sci* 265: 317–323. DOI: 10.1016/j.apsusc.2012.11.003
21. **Bosc F, Ayrat A, Albouy PA, Guizard C** (2003) A simple route for low-temperature synthesis of mesoporous and nanocrystalline anatase thin films, *Chem Mater* 15: 2463–2468. DOI: 10.1021/cm031025a
22. **Qi KH, Xin JH** (2010) Room-temperature synthesis of single-phase anatase TiO₂ by aging and its self-cleaning properties, *Appl Mater Interfaces* 2(12): 3479–3485. DOI: 10.1021/am1005892
23. **Gnauck M, Jaehne E, Blaettler T, Tosatti S, Textor M, et al.** (2007) Carboxy-terminated oligo(ethylene glycol)-alkane phosphate: synthesis and self-Assembly on titanium oxide surfaces, *Langmuir* 23(2): 377–381. DOI: 10.1021/la0606648
24. **Libanori R, Giraldi TR, Longo E, Leite ER, Ribeiro C** (2009) Effect of TiO₂ surface modification in Rhodamine B photodegradation, *J Sol-Gel Sci Technol* 49: 95–100. DOI: 10.1007/s10971-008-1821-1
25. **Chen K, Li JY, Wang WX, Zhang YM, Wang XJ, et al.** (2012) Effects of surfactants on microstructure and photocatalytic activity of TiO₂ nanoparticles prepared by the hydrothermal method, *Mater Sci Semicond Process* 15: 20–26. DOI: 10.1016/j.mssp.2011.05.007
26. **Liao L, Liao BQ** (2007) Shape, size and photocatalytic activity control of TiO₂ nanoparticles with surfactants, *J Photochem Photobiol A* 187: 363–369. DOI: 10.1016/j.jphotochem.2006.11.003
27. **Liao DL, Liao BQ** (2007) Shape, size and photocatalytic activity control of TiO₂ nanoparticles with surfactants, *J Photochem Photobiol A* 187: 363–369. DOI: 10.1016/j.jphotochem.2006.11.003
28. **Liao DL, Wu GS, Liao BQ** (2009) Zeta potential of shape-controlled TiO₂ nanoparticles with surfactants, *Colloids Surf. A* 348: 270–275. DOI: 10.1016/j.colsurfa.2009.07.036

29. **Oliveira EGL, Rodrigues JJ Jr, Oliveira HP** (2011) Influence of surfactant on the fast photodegradation of rhodamine B induced by TiO₂ dispersions in aqueous solution, *Chem Eng J* 172: 96–101. DOI: 10.1016/j.cej.2011.05.069
30. **Priya DN, Modak JM, Raichu AM** (2009) LbL fabricated poly(styrene sulfonate)/TiO₂ multilayer thin films for environmental applications, *Appl Mater Inter* 11(1): 2684–2693. DOI: 10.1021/am900566n
31. **Park BJ, Sung JH, Choi HJ** (2006) Electrophoretic TiO₂ nanoparticle modified with poly(methyl methacrylate), *J Electroceram* 17: 1031–1033. DOI: 10.1007/s10832-006-9242-4
32. **Linh NTB, Lee KH, Lee BK** (2011) Fabrication of photocatalytic PVA-TiO₂ nano-fibrous hybrid membrane using the electro-spinning method, *J Mater Sci* 46: 5615–5620. DOI: 10.1007/s10853-011-5511-y
33. **Kim JH, Shan WQ, Davies SHR, Baumann MJ, Masten SJ, et al.** (2009) Interactions of aqueous NOM with nanoscale TiO₂: Implications for ceramic membrane filtration-ozonation hybrid process, *Environ Sci Technol* 43: 5488–5494. DOI: 10.1021/es900342q
34. **Zahng QH, Gao L, Guo JK** (2000) Preparation and spectra characterization of quantum-size titanium dioxide in the rutile phase, *J Inorg Chem* 15(5): 931–932.
35. **Gao J, Tan XW, Miao YG, Xin RL** (2011) Modification of rutile nano-TiO₂ powders with visible light photocatalytic activity in hydrogen or nitrogen atmosphere, *Integrated Ferroelectrics* 129: 169–175. DOI: 10.1080/10584587.2011.576944
36. **Xu SB, Gu LX, Wu KH, Yang HG, Song YG, et al.** (2012) The influence of the oxidation degree of poly(3-hexylthiophene) on the photocatalytic activity of poly(3-hexylthiophene)/TiO₂ composites, *Sol. Energy Mater. Sol. Cells* 96: 286–291. DOI: 10.1016/j.solmat.2011.09.022
37. **Yin H, Wada Y, Kitamura T, Kambe S, Murasawa S, et al.** (2001) Hydrothermal synthesis of nanosized anatase and rutile TiO₂ using amorphous phase TiO₂, *J Mater Chem* 11: 1694–1703. DOI: 10.1039/b008974p
38. **Li K, Xiong JJ, Chen T, Yan LS, Dai YH, et al.** (2013) Preparation of graphene/TiO₂ composites by nonionic surfactant strategy and their simulated sunlight and visible light photocatalytic activity towards representative aqueous POPs degradation, *J Hazard Mater* 250–251: 19–28. DOI: 10.1016/j.jhazmat.2013.01.069
39. **Mogilevsky G, Chen Q, Kulkarni H, Kleinhammes A, Mullins WM, et al.** (2008) Layered nanostructures of delaminated anatase: nanosheets and nanotubes, *J Phys Chem C* 112: 3239–3246. DOI: 10.1021/jp076899p
40. **Song MX, Bian L, Zhou TL, Zhao XY** (2008) Surface ζ potential and photocatalytic activity of rare earths doped TiO₂, *J Rare Earths* 26(5): 693. DOI:10.1016/S1002-0721(08)60165-9
41. **Nieves AF, Nieves FJD** (1999) The role of ζ potential in the colloidal stability of different TiO₂: electrolyte solution interfaces, *Colloids Surf A* 148: 231–243. DOI:10.1016/S0927-7757(98)00763-8
42. **Wang H, Wang YL, Yan HK** (2006) Binding of sodium dodecyl sulfate with linear and branched polyethyleneimines in aqueous solution at different pH values, *Langmuir* 22: 1526–1533. DOI: 10.1021/la051988j
43. **Lu OY, Ramamoorthy M, Merlin LB** (2008) Multilayer polyelectrolyte films as nanofiltration membranes for separating monovalent and divalent cations, *J Membr Sci* 310: 76–84. DOI: 10.1016/j.memsci.2007.10.031
44. **Imae T, Muto K, Ikeda S** (1991) The pH dependence of dispersion of TiO₂ particles in aqueous surfactant solutions, *Colloid Polym Sci* 269: 43–48. DOI: 10.1007/BF00654658
45. **Weng Y, Li L, Liu Y, Wang L, Yang G** (2003) Surface-Binding Forms of Carboxylic Groups on Nanoparticulate TiO₂ Surface Studied by the Interface-Sensitive Transient Triplet-State Molecular Probe, *J Phys Chem B* 107: 4356–4363. DOI: 10.1021/jp022534n
46. **Ni M, Leung MKH, Leung DYC, Sumathy K** (2007) A review and recent developments in photocatalytic water-splitting using TiO₂ for hydrogen production. *Renewable Sustainable Energy Rev* 11: 401–425. DOI: 10.1016/j.rser.2005.01.009
47. **Francesca R, Bettini LG, Bahnemann DW, Sellì E** (2013) WO₃-TiO₂ vs. TiO₂ photocatalysts: effect of the W precursor and amount on the photocatalytic activity of mixed oxides, *Catal Today* 209: 28–34. DOI: 10.1016/j.cattod.2013.01.008

48. **Villoslada IM, Jofré M, Miranda V, Patricio C, González R, et al.** (2006) π -Stacking of rhodamine B onto water-soluble polymers containing aromatic groups, *Polymer* 47: 6496–6500. DOI:10.1016/j.polymer.2006.07.059
49. **Song HJ, Xiao HM, Dong HS** (2006) Density functional theory study of the properties of N-H \cdots N, noncooperativities, and intermolecular interactions in linear trans-diazene clusters up to ten molecules, *J Phys Chem A* 110: 6178–6183. DOI: 10.1021/jp061053r